Extreme Ultraviolet Application of Carbon Nanotube Structures

S. Olsen,[1] R. Vanfleet,[1, a)] D. Allred,[1, b)] S. Turley,[1, c)] and R. Davis[1, d)]
Brigham Young University

(Dated: 20 April 2020)

Windows for extreme ultraviolet (EUV) sources are challenging because of the lack of transparent materials in these wavelengths. Thus, differential pumping apertures and slits are standard. Our group has developed a carbon nanotube (CNT) window consisting of a dense array of square holes. The open area allows a large range of wavelengths to be transmitted, and the high density of holes restricts gas flow, allowing a large pressure difference with differential pumping. The versatility of CNTs allows us to select the peak transmission and pressure ratio (low/high). We have observed pressure ratios of 0.000924, 0.000667, 0.000494, and 0.00118 for air at 298 K with (width-heigth in microns) 50-301, 50-654, 50-1045, and 200-675, respectively for (high) pressures up to 1 torr.

I. INTRODUCTION AND BACKGROUND

A. Extreme Ultraviolet in Astrophysics

Extreme ultraviolet (EUV) observations have many applications in astrophysics. Spanning from 10 to 91.2 nm wavelength, common sources are divided into two categories: emission due to ion-electron recombination, and thermal emission. The former produces spectral lines, and include single or binary star systems with active coronae, hot O and B stars with winds, galaxy clusters, and the remnants of supernovae. The latter produces more of a continuum, and includes neutron stars, hot white dwarfs, and central stars of planetary nebulae. Thanks to several projects, such as the NASA Extreme Ultraviolet Explorer (EUVE), the UK Wide Field Camera (WFC), and the ALEXIS satellite, over 700 sources have been detected[1].

Due to most materials being absorptive to EUV[2], the WFC project used Wolter-Schwarzschild mirrors[3]; as well as the EUVE project[4]. Wolter-Schwarzschild mirrors are composed of several nested elliptical (or parabolic) mirrors and an outer hyperbolic one. Their design allows them to focus light by reflecting at grazing incidence[5], which increases reflectance. However, the design also limits the effective aperture, and has greater weight[5].

The ALEXIS project was unique in that it had a lightweight design with mirrors composed of multilayered coatings[1]. In a multilayered mirror, the materials and thicknesses of the layers are determined such that the reflections at each interface constructively interfere, resulting in a higher overall reflectance[2]. However, the materials and thicknesses are wavelength-dependent, therefore the bandpass of the mirror is greatly reduced. Therefore ALEXIS was not ideal for continuum spectra sources. An ideal mirror requires high reflectance at near-normal incidence (for a greater effective aperture) and a wide bandpass.

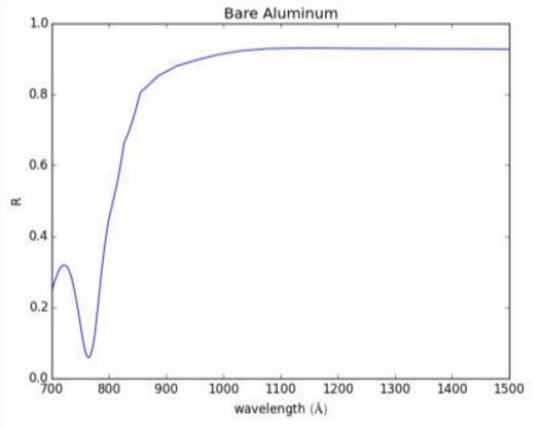

FIG. 1. Computed reflectance of a bare Al film on SiC at normal incidence[6].

B. Multilayered Mirror with Bare Al

Bare aluminum is theorized to permit such a mirror. Given its high reflectance at EUV wavelengths (shown in Figure 1), bare Al as a component in a two- and three- component multilayer mirror may allow high reflectance over a wide bandpass, as shown in Figure 2. However Al oxidizes easily, and the oxide layer reduces the reflectance[6]. This makes transportation and experimentation of a bare Al multilayered mirror difficult.

In experimentation, typical EUV sources are plasmas, which require a gas. If an Al mirror is placed in the same chamber as the plasma, the gas absorbs the EUV before it can reach the mirror. If any EUV did reach the mirror, the Al is already oxidized due to contaminants in the gas. Having the plasma and mirror in adjacent chambers with a glass (or any material) window would keep gas contaminants from oxidizing the Al, but then the window absorbs the EUV. Therefore testing a bare Al multilayered mirror requires a window that permits EUV while restricting gas flow.

C. Application of Carbon Nanotube Structure

We present a carbon nanotube (CNT) structure that provides the EUV throughput and gas flow restriction necessary for a bare Al mirror experiment.

[a)]Electronic mail: rrv3@byu.edu
[b)]Electronic mail: allred@byu.edu
[c)]Electronic mail: turley@byu.edu
[d)]Electronic mail: davis@byu.edu

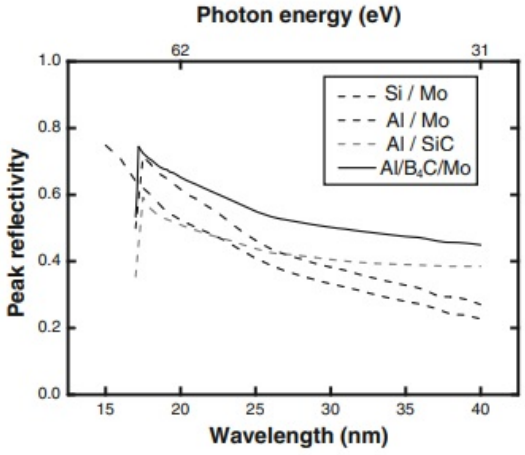

FIG. 2. Theoretical peak reflectivity of two- and three- component mirrors[2].

The versatility of CNTs make them a potential candidate for many applications involving high aspect ratio structures and MEMs. The technique allows for three-dimensional fabrication of many materials. The CNTs act as a framework, which when infiltrated with a material maintain their design, but exhibit the properties of the material, such as Young's modulus (with the exception of electrical conductivity)[7]. The versatility and high aspect ratio allow us to design a CNT collimator with properties required for a bare aluminum mirror experiment.

The structure design is an array of square open columns with the walls composed of CNT infiltrated with carbon. The open area permits EUV. The carbon infiltration is to make the structure more robust. The geometry of the structure will restrict gas flow, which maintains a pressure difference across the structure. This implies that a plasma can be run at a higher pressure on one side, while the mirror on the other side can be kept at a much lower pressure. Both the pressure difference and optical throughput depend on the width and height of the columns, which are easily determined during fabrication.

II. THEORY

The restriction on gas flow is modelled by calculating the conductance of the CNT structure; first by calculating the conductance of a single column, then the conductance of an array of columns. Assuming molecular flow regime, the conductance of the opening and length of the column are given in L/s by Eq. 1 and 2, respectively.

$$C_{opening} = 3.64w^2\sqrt{\frac{T}{M}} \tag{1}$$

$$C_{pipe} = 9.70\frac{w^3}{2h}\sqrt{\frac{T}{M}} \tag{2}$$

where T is temperature in Kelvin, M is the molecular weight of the gas in kg/mol, h and w are the height and width of the column in cm, respectively[8]. Adding the two conductances in series gives the conductance of one column:

$$C_{column} = \frac{1}{\frac{1}{C_{opening}} + \frac{1}{C_{pipe}}} \tag{3}$$

Then multiply by the number of columns to obtain the conductance of a structure with area A:

$$C_{structure} = N_{columns}C_{column} \approx \frac{A}{A_{column}}C_{column} = \frac{AC_{column}}{(w+t)^2} \tag{4}$$

Assuming the thickness of the walls (t) is much less than the pore size (w), the conductance is approximately:

$$C_{structure} \approx \frac{AC_{column}}{w^2} = \frac{A}{0.275 + 0.206\frac{h}{w}}\sqrt{\frac{T}{M}} \tag{5}$$

The pressure ratio across the structure is given by:

$$\frac{P_L}{P_H - P_L} = \frac{C}{S} \tag{6}$$

Where S is the pumping speed in L/s, and P_L and P_H are the low and high pressures in torr, respectively[8]. The result is:

$$\frac{P_L}{P_H - P_L} = \frac{1}{S} * \frac{A}{0.275 + 0.206\frac{h}{w}}\sqrt{\frac{T}{M}} \tag{7}$$

A. CNT Fabrication

CNT structures were grown using a procedure similar to the one outlined in Hutchison, et al. These steps include:

- Photolithography of structure pattern using AZ3330 photoresist on a Al2O3 wafer
- Deposition of a 4 nm iron layer by thermal evaporation onto wafer
- Liftoff of photoresist using Microposit 1165
- CNT growth in quartz tube furnace using atmospheric CVD with ethene, followed by carbon infiltration.
- Plasma etching with an oxygen plasma at 200 W and 0.4 atm for 5 min for top and bottom

III. EXPERIMENTATION

Experimentation is divided into two stages of testing: pressure ratio with room temperature air, pressure ratio and optical throughput with a helium plasma and EUV.

A. Pressure Ratio With Room Temperature Air

The test involved mounting the CNT structure between two chambers at different pressures. As the pressure in one chamber was varied (P_H), the pressure in the other was observed (P_L).

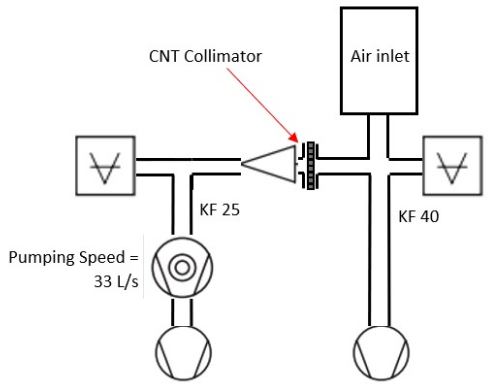

FIG. 3. Experiment setup for CNT structure pressure ratio.

B. Setup

Figure 3 shows the pressure ratio setup. The two chambers were two KF cross-connectors. Both were connected to individual turbomolecular pumps, backed by a roughing pump. The P_H cross-connector had a baratron; the P_L had a ion gauge. The P_H also included a controlled-leak valve. A CNT structure was mounted to a KF40 2 mm orifice restrictor using epoxy, and placed between the connectors. The chambers pumped till pressures were stable. Then the turbomolecular pump of the P_H was turned off, and the leak opened. P_H was increased incrementally; P_L observed. Pressures were kept close or under 1 torr to maintain molecular flow regime.

C. Data and Discussion

CNT structures tested are listed in Table I. Heights were measured in a SEM. To account the for the conductance of the 2mm orifice restrictor, two trials were conducted with the restrictor with no CNT structure mounted (Figure 4). Given the pumping speed of $S = 33$L/s for the turbomolecular pumps, the conductance of the restrictor was calculated to be 0.0625±0.0101 L/s. Adding in series this conductance to the CNT structure conductance calculated using Eq 5 with $A = 3.14$mm squared and $\sqrt{T/M} = 3.214$ for air at room temperature, then dividing by S, we have the predicted pressure ratios, listed in Table I. Observed pressure ratios were calculated by taking the average of data points above a pressure ratio of 0.2 torr for all trials. The incline below 0.2 torr may be due to leaks in the system becoming more significant as the controlled leak is decreased. Error is calculated using standard deviation.

Figure 5 shows the pressure ratio of the CNT structures mounted to the 2mm orifice restrictor. Notice that the predicted pressure ratio for D is significantly higher than the observed ratio. This may be due to the approximation in Eq 4- this approximation becomes less valid as the width of the structure pores increases. As w increases, a greater portion of a pore's square open area is overlapped with the circular orifice. The increase in overlap effectively decreases $C_{opening}$,

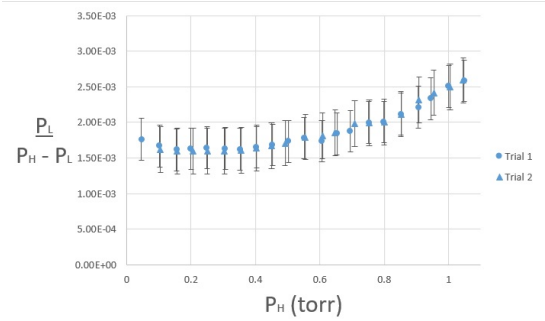

FIG. 4. Observed pressure ratio due to 2mm orifice restrictor. Errors bars are standard deviation of points within a given trial.

Structure	Width (microns)	Height (microns)	Pressure Ratio (10^{-4}) Predicted	Observed
A	50	301	9.774	9.24±0.436
B	50	654	6.67	6.24E±0.352
C	50	1045	4.94	4.46±0.270
D	200	675	11.8	10.3±0.200

TABLE I. Predicted and observe pressure ratios of various CNT structures tested with air at room temperature. Note the tendency for the predicted to be higher than the observed. This may be due to the approximation in Eq 4, with structure D being the extreme example.

which decreases $C_{structure}$, which decreases the pressure ratio.

D. EUV

Unlike the previous experiments, the EUV experiment intends to demonstrate the CNT structure's application in testing a bare aluminum mirror more directly in that it involves EUV throughput and restricting gas flow from a plasma. Both throughput and pressure ratio will be observed simultaneously.

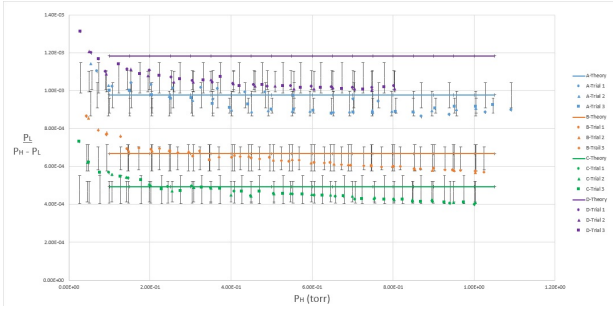

FIG. 5. Observed pressure ratio across CNT structures mounted to a 2 mm restrictor. Structures of different width-height are differentiated by color; trials are differentiated by symbol. Lines are theory using Eq 7. Error bars are calculated using standard deviation based on data within a given trial.

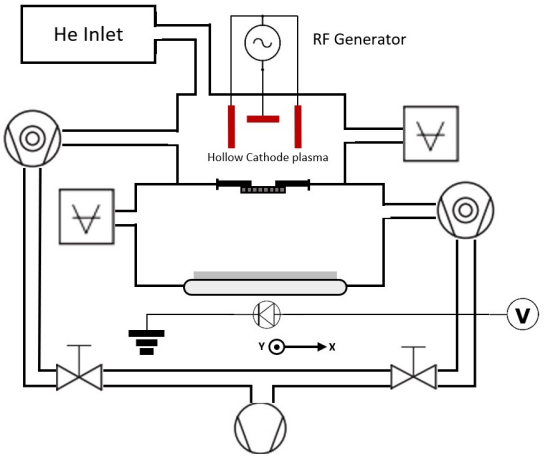

FIG. 6. Experiment setup of EUV experiment.

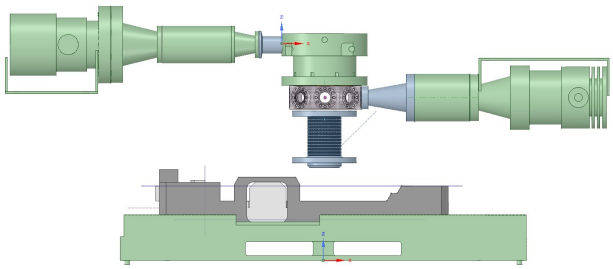

FIG. 7. Current EUV Experiment design. Note the replacement of the lower chamber with a bellows mounted to an xy table for practicality. Phosphur window, photodiode, and pressure gauges are not shown.

E. Setup

Figure 6 shows the setup of the experiment. The experiment involves two chambers, each connected to pumps and pressure gauges. In the upper chamber is a hollow cathode plasma. The lower includes a window coated with a phosphur. Under the lower chamber is a photodiode mounted to a xy table. A CNT structure is mounted to an aperture between the two chambers. The pressure gauges observe the pressure ratio between the chambers. EUV from the plasma through the structure illuminates the phosphur-coated window. The photodiode moving across the xy table recordes the illumination of the phosphur, observing the EUV throughput.

Figure 7 is the experiment currently . The plasma anode is the central green solid, run at 800 V with variable pressure up to 1 torr. Turbomolecular pumps to the side of the anode and the lower chamber have a pumping speed of 55 L/s. Micro-Pirani gauges (not shown in diagram) with a range of 10^{-5} to 760 torr will be used. The lower chamber includes a bellows which is mounted to the xy table externally. The photodiode (not shown) is designed to respond to visible wavelengths between 188 microlumens and 220 kilolumens. The xy table has a range of 39 mm by 33 mm.

Given the range of the xy table and the height of the plasma anode above it, the experiment is limited to a scanning angle of about 3.7 degrees. Note also that the aperture the CNT structure will be mounted to will also restrict EUV throughput. Restricting the structure's throughput to less than that of the aperture and scanning angle; using Eq 7 with $\frac{P_L}{P_H - P_L} = \frac{1}{9}$, $S = 55$, $A = \pi * r^2$ where r is the radius of the aperture in cm, $T = 300 \leftrightarrow 500$ K, and $M = 0.0040026$ kg/mol for helium; and solving for h with set values for w, we obtain the values listed in Table II:

Width (microns)	Height (microns)	θ_c (degrees)	Radius (cm)
25	$511 \leftrightarrow 557$	$3.11 \leftrightarrow 2.86$	$0.179 \leftrightarrow 0.157$
50	$1022 \leftrightarrow 1115$	$3.11 \leftrightarrow 2.85$	$0.13 \leftrightarrow 0.114$
100	$2044 \leftrightarrow 2230$	$3.11 \leftrightarrow 2.85$	$0.097 \leftrightarrow 0.085$
200	$4089 \leftrightarrow 4460$	$3.11 \leftrightarrow 2.85$	$0.075 \leftrightarrow 0.066$

TABLE II. CNT structure dimensions necessary for maximum pressure ratio within limiting aperture and scanning angle.

Due to difficulty in growing CNTs above 1100 microns, we restrict the experiment to only 25 and 50 micron width structures. Note that these values are calculated for the maximum pressure ratio desired. Therefore structures of same w and larger h are also considered. The apertures for the 25 and 50 micron CNT structures are 3.175 mm thick, and have a diameter of 3.25 and 2.35 mm, respectively.

Given only 25 and 50 micron pores will be used on apertures larger than the 2mm orifice restrictor mentioned previously, we consider the approximation in Eq 4 to be valid.

IV. CONCLUSION

We have presented a CNT structure as an ideal window for testing the EUV reflectance of a bare aluminum mulitlayer mirror at near-normal incidence. Versatility of CNTs allow the structure to meet the experiment's requirements. The structure's design allows for EUV throughput while restricting gas flow- slowing the rate of oxidation in the mirror. Gas flow restriction have been observed for air and room temperature. We intend to demonstrate its application further by observing its EUV throughput and restriction of helium gas flow from a plasma.

ACKNOWLEDGMENTS

We wish to acknowledge the support of BYU's Physics and Astronomy Department for funding, John Ellsworth for experiment design, the BYU Microscopy Department for providing the SEM images, BYU IMF for providing the photolithography equipment, and the BYU Physics Machine Shop for fabrication of necessary components.

[1] M. A. Barstow, S. L. Casewell, J. B. Holberg, and M. P. Kowalski, "The status and future of euv astronomy," Advances in Space Research **53**, 1003–1013 (2014).

[2] C. Bourassin-Bouchet, S. de Rossi, and F. Delmotte, "Multilayer mirrors for coherent extreme-ultraviolet and soft x-ray sources," in *Optical Technologies for Extreme-Ultraviolet and Soft X-ray Sources*, Springer Series in Optical

Sciences, Vol. 197, edited by F. Canova and L. Poletto (McGraw-Hill, 2015) Chap. 8, pp. 151–173.

[3]R. Warwick, "Euv astronomy with the rosat wide field camera," in *Frontiers of Space and Ground-based Astronomy: The Astrophysics of the 21st Century*, edited by W. Wamsteker, M. Longair, and Y. Kondo (Springer Netherlands, Dordrecht, 1994) pp. 57–66.

[4]M. Sirk, J. Vallerga, D. Finley, P. Jelinsky, and R. Malina, "Performance of the extreme ultraviolet explorer imaging telescopes," The Astrophysical Journal Supplement Series, **110**, 347–356 (1997).

[5]M. Arndt Last, *Curved mirror optics*, http://www.x-ray-optics.de/index.php/en/types-of-optics/reflecting-optics/curved-mirrors, Accessed 3/24/2020.

[6]D. D. Allred, R. S. Turley, S. M. Thomas, S. G. Willett, M. J. Greenburg, and S. B. Perry, "Adding euv reflectance to aluminum-coated mirrors for space-based observation," in *UV/Optical/IR Space Telescopes and Instruments: Innovative Technologies and Concepts VIII*, Vol. 10398, edited by H. A. MacEwen and J. B. Breckinridge, International Society for Optics and Photonics (SPIE, 2017) pp. 345–362.

[7]D. N. Hutchison, N. B. Morrill, Q. Aten, B. W. Turner, B. D. Jensen, L. L. Howell, R. R. Vanfleet, and R. C. Davis, "Carbon nanotubes as a framework for high-aspect-ratio mems fabrication," Journal of Microelectromechanical Systems **19**, 75–82 (2010).

[8]M. Ohring, *Materials Science of Thin Films* (Academic Press, 2002) Chap. 2.